Supporting Information

Brown et al. 10.1073/pnas.1217338109

SI Materials and Methods

β-Globin Reporter Assays. HEK293T cells were grown in Dulbecco's modified Eagle medium (Life Technologies) supplemented with 10% FBS (vol/vol), 2 mM L-glutamine, and 1× penicillin streptomycin solution. Transfections were performed using TransIT-293 (Mirus) per the manufacturer's protocol. Cells were harvested 24–48 h after transfection, and RNA was isolated using TRIzol (Life Technologies). Ten micrograms of total RNA was loaded onto a 1.2% agarose (wt/vol)/6.5% formaldehyde (vol/vol) gel, resolved overnight at 70 V, and transferred to a Zeta-Probe GT blotting membrane (Bio-Rad) via upward capillary transfer with 20× SSC. Three DNA oligonucleotides (Integrated DNA Technologies) were 5′-[^{32}P]-labeled to detect NeoR mRNA (5′-GCATCAGAGCAGCCGATTGTCTGTTG-3′, 5′-GCATCAGCCATGATGGATACTTTCTCGG-3′, and 5′-CGGCCATTTTCCACCATGATATTCGGCAAGC-3′) and a uniformly [^{32}P]-labeled antisense RNA probe was used to detect β-globin mRNA. To calculate the level of β-globin mRNA accumulation, the β-globin signal was divided by the signal for the NeoR mRNA, which served as a loading and transfection control because it is encoded on the same plasmid as the β-globin reporter. Then, all values were normalized relative to βΔ1,2 lacking an insert, which was set at an arbitrary value of 1, and mutants were normalized relative to the appropriate WT counterpart.

RNA Preparation. RNA oligonucleotides A_9GCA_4, $CAG_2A_5GCA_4$, and A_{15} (Dharmacon) were deprotected and dried according to the manufacturer's instructions and resuspended in ddH_2O. For gel-shift assays, the metastasis-associated lung adenocarcinoma transcript 1 (MALAT1) (nucleotides 8263–8328) and multiple endocrine neoplasia-β (MENβ) (nucleotides 22649–22710) expression and nuclear retention elements (ENEs) were transcribed by his-tagged T7 RNA polymerase using a PCR-generated template, and the RNA product was processed as described previously (1), except the RNA was resuspended in ddH_2O and aliquoted before storage. To enhance transcription, the template was altered to start with GG. For UV melting studies, the RNA was transcribed and processed as described above except DraI-linearized pHDV plasmids served as templates.

Gel-Shift Assays. RNA oligonucleotides were 5′-[^{32}P]-labeled using γ-[^{32}P]ATP (PerkinElmer) and T4 PNK (New England Biolabs) per the manufacturer's protocol. Free γ-[^{32}P]ATP was removed by passing the reaction mixture through a Microspin G-25 column (GE Healthcare). Increasing concentrations of the ENE were titrated into the equilibration solution, which contained 25 mM sodium cacodylate pH 7, 50 mM KCl, 1 mM $MgCl_2$, 0.5 mg/mL yeast tRNA, 10% glycerol (vol/vol), and 2 nM 5′-[^{32}P]-labeled oligonucleotide. The mixture was heated at 95 °C for 3 min, snap-cooled on ice for 10 min, and allowed to equilibrate at room temperature for 1 h. Then, the binding reaction was resolved on an 8% native (vol/vol) Tris-acetate gel with 1 mM $MgCl_2$ in the gel and running buffer. After electrophoresis for 1.5–2 h at 150 V and room temperature, the gels were dried, exposed to a phosphorimager screen overnight, and scanned using a Storm 860 (GE Healthcare).

SI Discussion

For the data presented in Fig. 1*C*, it was somewhat surprising that the βΔ1,2-MALAT1/MENβ ENE+A reporters (Fig. 1*C*, lanes 5 and 15) did not exhibit stabilization activity despite the presence of a transcript having an ENE and an A-rich tract that contains GC, both of which were shown to be important from the assays presented in Fig. 3. However, transcript stabilization occurs when mascRNA or menRNA are added to βΔ1,2-MALAT1/MENβ ENE+A, raising the question: What are the roles of RNase P and the tRNA-like sequences in transcript stabilization? Although we do not fully understand the relationship between stabilization activity in vivo and the presence of mascRNA or menRNA inducing transcript cleavage by RNase P, it is clearly important to have a 3′ blunt-ended triplex without unpaired nucleotides at the duplex-triplex junction as shown in Fig. 3*B*. The uncleaved transcripts of βΔ1,2-MALAT1 ENE+A or βΔ1,2-MENβ ENE+A (Fig. 1*C*, lanes 5 and 15) would have nucleotide overhangs at the 3′ end, which could create a binding site for an exonucleolytic enzyme to initiate degradation of the transcript. However, our results do not exclude RNase P from having a possible role in stabilization activity, such as chaperone-like activity to assist with formation of an ENE-like structure. To determine if having a free 3′ end is important for stabilization activity independent of RNase P cleavage, we have engineered and tested βΔ1,2 reporters with alternative 3′-end processing mechanisms, whereby the tRNA-like structure was replaced with a *cis*-acting ribozyme (HDV or hammerhead). None of these mutant constructs exhibited stabilization activity, so it remains unclear whether such negative results are because of inefficient processing or the absence of RNase P. Another possibility, which we have not investigated, is that the mascRNA or menRNA structure facilitates the folding of an ENE-like structure. Additional studies are needed to address these important mechanistic questions.

1. Mitton-Fry RM, DeGregorio SJ, Wang J, Steitz TA, Steitz JA (2010) Poly(A) tail recognition by a viral RNA element through assembly of a triple helix. *Science* 330(6008):1244–1247.

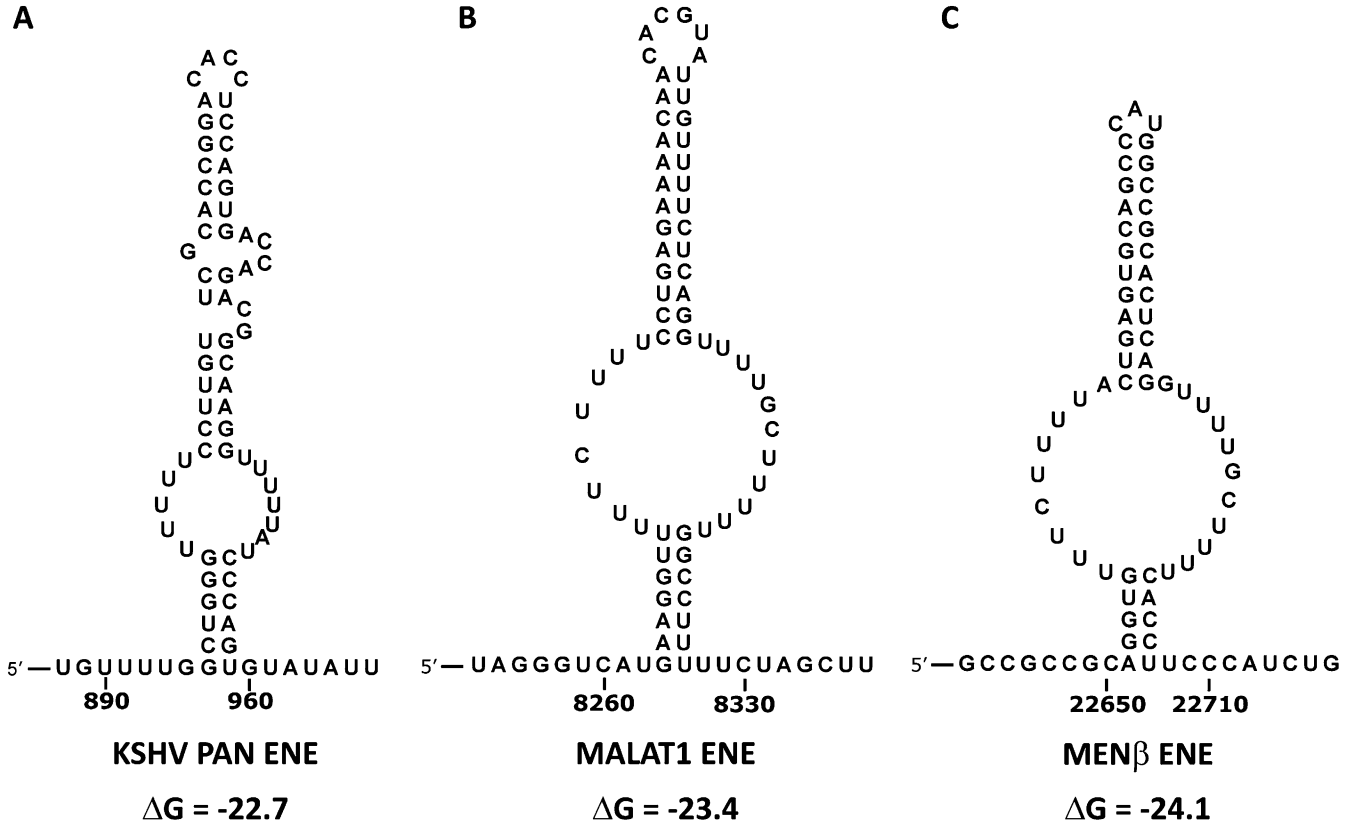

Fig. S1. Secondary structure predictions using Mfold. Predicted secondary structures are shown for (*A*) Kaposi's sarcoma-associated herpesvirus (KSHV) polyadenylated nuclear (PAN) ENE, (*B*) putative MALAT1 ENE, and (*C*) putative MENβ ENE, all of which are the same sequences inserted into the βΔ1,2 reporter constructs. The ΔG values are in units of kilocalorie per mole from the Mfold program (1) and exclude the unpaired 5′- and 3′-flanking sequences beneath the lower stem.

1. Zuker M (2003) Mfold web server for nucleic acid folding and hybridization prediction. *Nucleic Acids Res* 31(13):3406–3415.

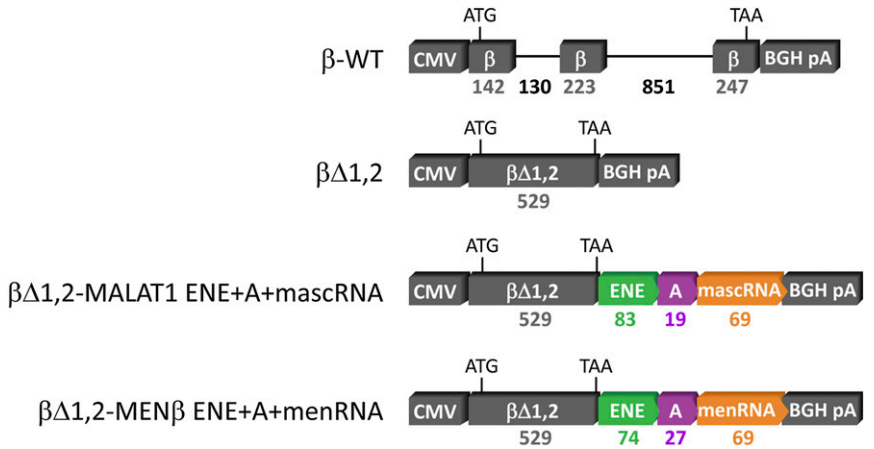

Fig. S2. Detailed schematics of select β-globin reporter plasmids. In the pcDNA3 vector (Invitrogen), all β-globin sequences (β) are flanked by a human CMV immediate-early promoter at the 5′ end and a bovine growth hormone polyadenylation signal (BGH pA) at the 3′ end. Both the β-WT (with introns) and βΔ1,2 (intronless) reporter plasmids have been described previously (1, 2). Briefly, the β-WT reporter contains two introns (black lines) and three exons (boxes). PCR inserts of the MALAT1 and MENβ sequences were inserted into the 3′ UTR at the ApaI site, which is located 137 nts upstream from the BGH pA signal of AATAAAA. Insert sizes for MALAT1 are as follows: 83 nts for the predicted ENE (Fig. S1*B*), 19 nts for the A-rich tract, and 69 nts for mascRNA. Insert sizes for MENβ are as follows: 74 nts for the predicted ENE (Fig. S1*C*), 27 nts for the A-rich tract, and 69 nts for menRNA. Note, the βΔ1,2 constructs have a Flag-tag at the N terminus (not shown) and encode the Neomycin resistance gene (not shown), the transcript of which served as a transfection and loading control. Boxes and lines are not drawn to scale.

1. Lykke-Andersen J, Shu MD, Steitz JA (2000) Human Upf proteins target an mRNA for nonsense-mediated decay when bound downstream of a termination codon. *Cell* 103(7): 1121–1131.
2. Conrad NK, Steitz JA (2005) A Kaposi's sarcoma virus RNA element that increases the nuclear abundance of intronless transcripts. *EMBO J* 24(10):1831–1841.

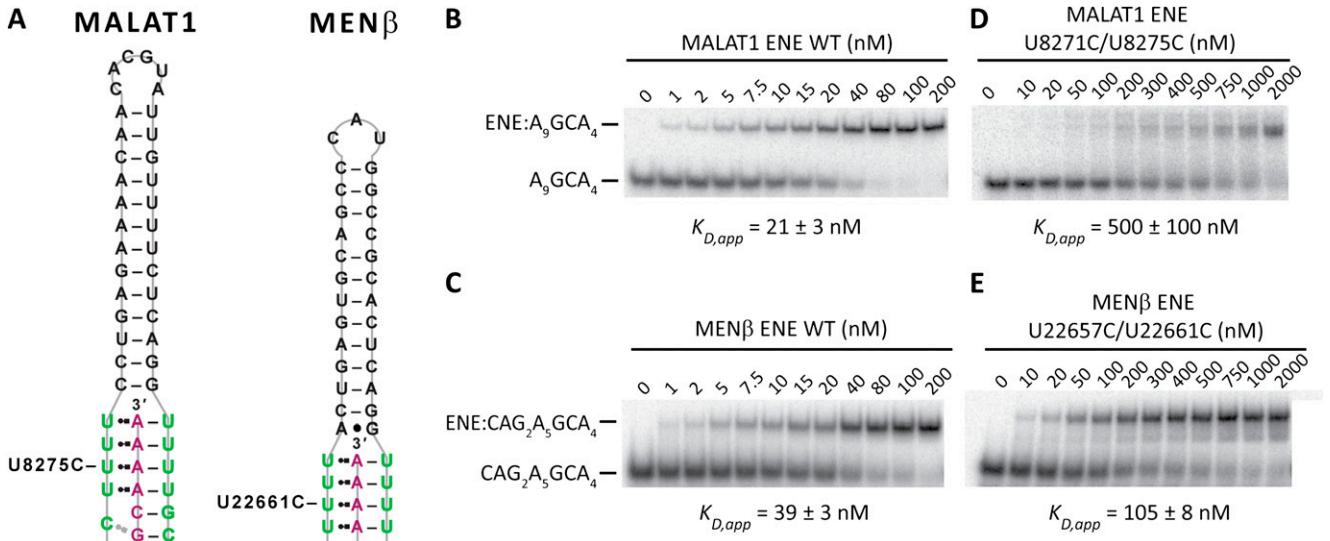

Fig. S3. The predicted MALAT1 and MENβ ENEs interact strongly with A-rich oligonucleotides in *trans*. (*A*) Schematic diagrams are shown for the predicted ENE-like structures from MALAT1 (nucleotides 8263–8328) and MENβ (nucleotides 22651–22709) interacting with an A-rich oligonucleotide (5′-A_9GCA_4-3′ for MALAT1 and 5′-$CAG_2A_5GCA_4$-3′ for MENβ). Predicted interactions are the same as shown in Fig. 1*A*. Green denotes the U-rich internal loop and purple denotes the A-rich tract. Mutants with double U-to-C substitutions are indicated. Nonnative nucleotides are in gray. (*B–E*) Gel-shift assays were performed by adding increasing concentrations of the putative ENE to the appropriate 5′-[^{32}P]-labeled A-rich oligonucleotide (2 nM): (*B*) MALAT1 ENE WT + 5′-A_9GCA_4-3′, (*C*) MENβ ENE WT + 5′-$CAG_2A_5GCA_4$-3′, (*D*) MALAT1 ENE U8271C/U8275C + 5′-A_9GCA_4-3′, and (*E*) MENβ ENE U22657C/U22661C + 5′-$CAG_2A_5GCA_4$-3′. The RNA was folded and allowed to equilibrate for 1 h at room temperature before separating the ENE:A-rich oligonucleotide complex from the unbound oligonucleotide using native polyacrylamide gel electrophoresis. Apparent equilibrium dissociation constants ($K_{D,app}$) were extracted by fitting a quadratic equation, $[E{\cdot}O] = 0.5(K_{D,app} + E_0 + O_0) - 0.5[(K_{D,app} + E_0 + O_0)^2 - 4E_0O_0]^{1/2}$, to plots of ENE:oligonucleotide complex versus the concentration of ENE using Kaleidagraph software. E_0 and O_0 represent the ENE and oligonucleotide concentrations, respectively. $K_{D,app}$ values are the average of three independent measurements ± SD.

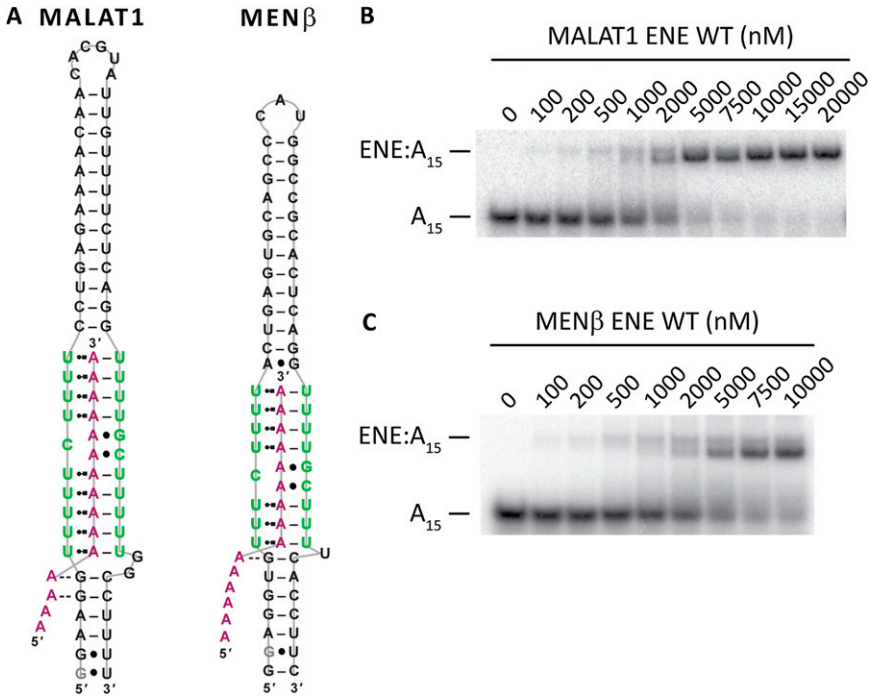

Fig. S4. The predicted MALAT1 and MENβ ENEs interact weakly with oligo(A_{15}) *in trans*. (*A*) Schematic diagrams are shown for the predicted ENE-like structures from MALAT1 (nucleotides 8263–8328) and MENβ (nucleotides 22651–22709) interacting with oligo(A_{15}). Nomenclature for predicted interactions is defined in Fig. 1*A*. Green denotes the U-rich internal loop and purple denotes oligo(A_{15}). Nonnative nucleotides are in gray. (*B* and *C*) Gel-shift assays were performed by adding increasing concentrations of the putative (*B*) MALAT1 ENE WT (100-20,000 nM) or (*C*) MENβ ENE WT (100–10,000 nM) to 5′-[^{32}P]-labeled oligo(A_{15}) (2 nM). The RNA was folded and allowed to equilibrate at room temperature for 1 h before separating the ENE:A_{15} complex from the unbound oligonucleotides using native polyacrylamide gel electrophoresis.

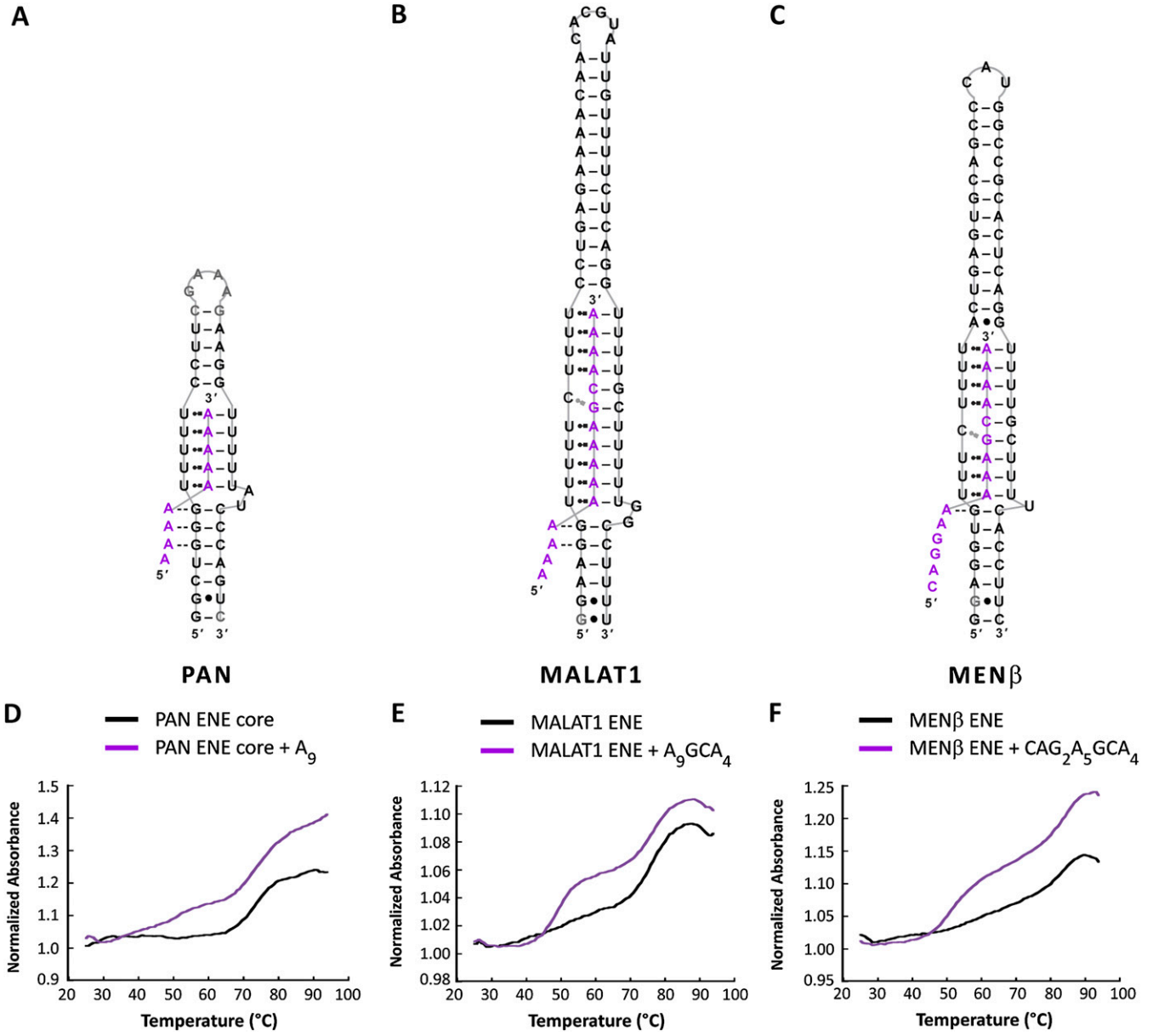

Fig. S5. UV melting profiles for predicted ENEs with and without an A-rich oligonucleotide. UV thermal denaturation experiments were performed using a bimolecular (or interstrand) system to verify that the first transition is observed only when the ENE interacts with the appropriate A-rich oligonucleotide. (*A–C*) Schematic diagrams of the predicted ENEs (black) are complexed with the appropriate A-rich oligonucleotide (purple) as in Fig. 1*A*. Nonnative nucleotides are in gray. The secondary and tertiary interactions for the PAN ENE core:A_9 complex in (*A*) were established by X-ray crystallography (1). (*D–F*) Plots of normalized absorbance at 260 nm versus temperature are shown for (*D*) PAN ± A_9, (*E*) MALAT1 ± A_9GCA_4, and (*F*) MENβ ± $CAG_2A_5GCA_4$. The black lines represent denaturation of the ENE alone and the purple lines represent denaturation of the ENE + A-rich oligonucleotide. Melting temperatures were not extracted from these data because values shift depending on the concentrations of each RNA molecule (2).

1. Mitton-Fry RM, DeGregorio SJ, Wang J, Steitz TA, Steitz JA (2010) Poly(A) tail recognition by a viral RNA element through assembly of a triple helix. *Science* 330(6008):1244–1247.
2. Lee HT, Arciniegas S, Marky LA (2008) Unfolding thermodynamics of DNA pyrimidine triplexes with different molecularities. *J Phys Chem B* 112(15):4833–4840.

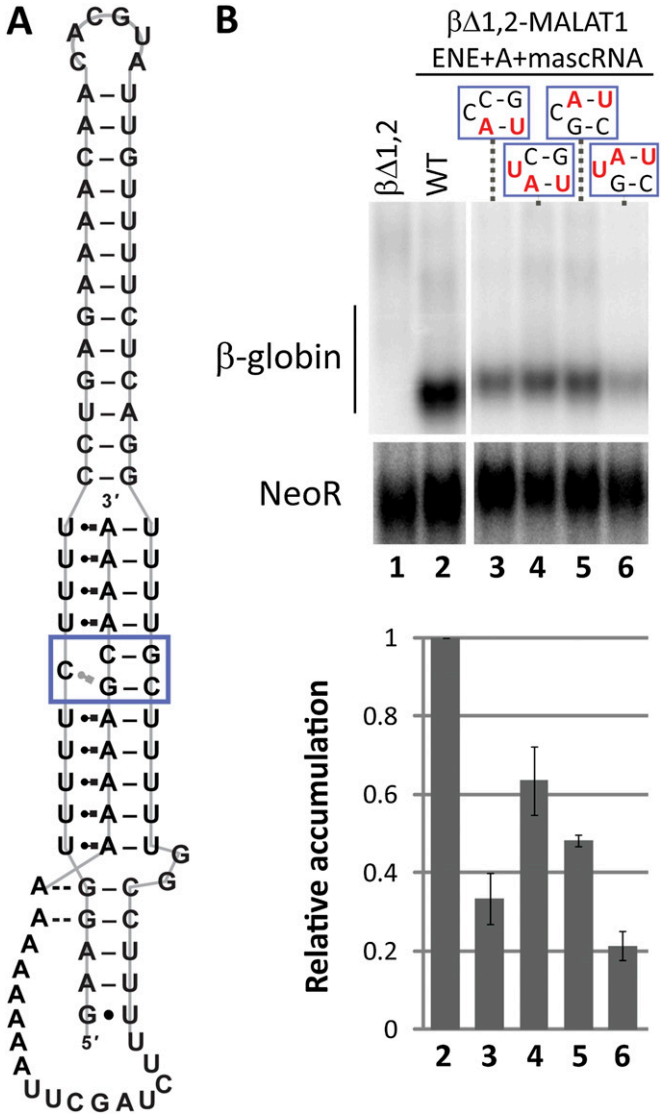

Fig. S6. Intervening C and G nucleotides in the U-rich loop likely form a C•G-C triple. (*A*) The same schematic diagram as in Fig. 1*A* shows the predicted ENE-like structure for MALAT1 (nucleotides 8263–8355). The blue box outlines the region targeted for mutagenesis. (*B*) Northern blot analysis of β-globin and NeoR mRNAs (*Upper*) and quantitation (*Lower*) were performed as in Fig. 1*C*. Black nucleotides are WT sequence and mutated nucleotides are red. The WT βΔ1,2 reporter level was set at an arbitrary value of 1. Relative accumulation is the average of at least three independent experiments and error bars represent SD.